Vol 13 No 6, June 2004
1009-1963/2004/13(06)/0958-10

Chinese Physics

© 2004 Chin. Phys. Soc.
and IOP Publishing Ltd

Phase separation and abnormal transport behaviours in $La_{0.7-x}Gd_xSr_{0.3}MnO_3$ system*

Liu Ning(刘 宁)[a)b)†], Tong Wei(童 伟)[b)], and Zhang Yu-Heng(张裕恒)[b)]

[a)] *Department of Physics, Suzhou Advanced Normal College, Suzhou 234000, China*

[b)] *Structure Research Laboratory, University of Science and Technology of China, Hefei 230026, China*

(Received 24 September 2003; revised manuscript received 12 February 2004)

The magnetic and transport behaviours of the $La_{0.7-x}Gd_xSr_{0.3}MnO_3$ ($0 \leq x \leq 0.70$) system are investigated. The experimental results indicate that with increasing Gd doping content, the magnetism of the system changes from the long-range ferromagnetic order state to the cluster-spin glass state, then to the antiferromagnetic (AFM) state. It is interesting that the phase separation appears at x=0.30 and 0.40 and disappears for $x \geq 0.50$ where the AFM state occurs. At high doping content, the transport behaviours exhibit abnormality, e.g. there are two temperature ranges in which the ρ–T curves can be well fitted by a variable-range hopping (VRH) model. We suggest that the VRH does not come from the hopping of carriers between clusters, but from the different magnetic backgrounds in the clusters.

Keywords: magnetic structure, phase separation, abnormal transport behaviours
PACC: 7550L, 7210

1. Introduction

In 1993, Helmolt *et al*[1] discovered the colossal magnetroresistance (CMR) effect in $La_{2/3}Ba_{1/3}MnO_3$ film, which has attracted much attention. It is widely accepted that the transport mechanism is dominated by double-exchange (DE) interaction and the Jahn–Teller (JT) effect, but different doping elements lead to different electric and magnetic behaviours. Generally, the doping at the A site causes the Curie temperature T_C to decrease, and a paramagnetism–ferromagnetism (PM–FM) transition takes place accompanied by an insulator–metal (IM) transition, with the CMR effect appearing mostly near the PM–FM transition. With increasing doping content, the cluster-spin glass state appears,[2–4] a random Coulomb potential and magnetic fluctuating potential are created, and the transport mechanism changes from small polaron activation to variable-range hopping (VRH).[2–6] The doping at the B site directly destroys DE interaction, and the PM–FM transition often occurs without the appearance of IM transition. The magnetic ion Cr^{3+}-doping at the B site leads to the appearance of PM–FM transition without that of IM transition. Sun *et al*[6] indicated that because the electronic configuration of Cr^{3+} is the same as that of Mn^{4+} and both are $t_{2g}^3\ e_g^0$, it is possible that there is a DE interaction between Cr^{3+} and Mn^{3+}.

In this paper we study the electric and magnetic behaviours of the system $La_{0.7-x}Gd_xSr_{0.3}MnO_3$ ($0 \leq x \leq 0.70$). Experimental results show that with increasing Gd doping content, the magnetism of the system changes from the long-range FM order state to the cluster-spin glass state and antiferromagnetic (AFM) state, and phase separation appears in the cluster-spin glass state; moreover, at high doping content, the transport behaviour becomes abnormal because the carriers move during the phase separation and in the AFM magnetic background.

2. Experiment

The polycrystalline samples $La_{0.7-x}Gd_xSr_{0.3}MnO_3$ (x=0.00, 0.10, 0.15, 0.20, 0.30, 0.40, 0.50, 0.60 and 0.70) were prepared by a conventional solid-state reaction method. Stoichiometric proportions of high-purity powders of La_2O_3, $SrCO_3$, Gd_2O_3, and MnO_2 were mixed and first fired at 900 °C for 12 h. Then the mixture was heated at 1000 °C for 12 h and at 1200 °C for 24 h to gain a crystalline state.

*Project supported by the National Natural Science Foundation of China (Grant No 10334090) and the State Key Development Programme for Basic Research of China (Grant No 001CB610604).

†E-mail: liuning.szsz@163.com

Finally, the mixed powders, pressed into pellets, were reacted at 1400 °C for 24 h in oxygen atmosphere.

X-ray diffraction (XRD) was carried out with a Rigaku-D/max-γA diffractometer using high-intensity Cu-$K\alpha$ radiation to detect the presence of impurity phase and the changes in structure. Magnetization measurements were carried out using a Lakeshore vibrating sample magnetometer (VSM). The measurements were achieved in warming condition after cooling the sample in zero field or 0.01 T magnetic field to 5 K. The M–H curves were also measured using the VSM. The electron spin resonance (ESR) experiments were carried out with a BRUKER ER-200D ESR spectrometer, with the microwave frequency being 9.61 GHz, and the measured spectra were the microwave absorption spectra in a temperature range from 100 to 400 K. The resistivity was measured using the standard four-probe method in a closed-cycle helium cryostat under zero field (H=0 T) and magnetic field (H=1 and 6 T). The applied magnetic field was perpendicular to the electrical current, and the measuring electrical current was kept at a certain value between 1 and 10 mA according to the value of the resistivity of the samples.

3. Results and discussion

Figure 1 gives the powder XRD patterns of all the samples. The calculated diffraction intensity and the peak position are in good accordance with the experimental results, and no extra peaks appear. This indicates obviously that the mean structure of the samples does not show structural change even when the Gd doping content increases to x=0.70. The XRD results indicate that all the samples are crystallized in single phase with ABO_3 structure.

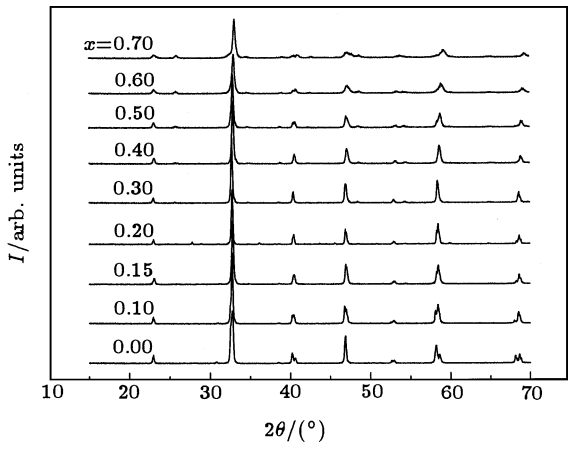


Fig.1. XRD patterns of powder samples of $La_{0.7-x}Gd_xSr_{0.3}MnO_3$.

3.1. The long-range FM order state, the cluster-spin glass state, and the AFM state

The M–T curves of all the samples are shown in Fig.2, from which we can see that the magnetic moment of the system decreases with increasing doping content, and the sample exhibits three types of magnetic structure: (1) for $x \leq 0.20$, the M–T curves under zero field cooling (ZFC) are basically in accordance with those under field cooling (FC). The transition from PM to FM state is very sharp. The system exhibits a typical FM behaviour (that is, the long-range FM order state) after this transition; (2) for x=0.30 and 0.40, the M–T curves under ZFC are obviously different from those under FC below T_C (Curie temperature T_C is defined as the temperature corresponding to the minimum of dM/dT in the M–T curve), and the system exhibits the cluster-spin glass behaviour; (3) for $x \geq 0.50$, the M–T curves under both ZFC and FC drop rapidly with decreasing temperature below T_C, and the system exhibits AFM behaviour. For x=0.50, the magnetization under FC decreases with increasing temperature at $T > 20$ K (which is in accordance with that of samples with x=0.30 and 0.40), but the magnetization under ZFC and FC increases with increasing temperature for $T < 20$ K (which is in accordance with that of samples x=0.60 and 0.70 at low temperatures). So the sample with x=0.50 shows a transition from cluster-spin glass state to AFM state.

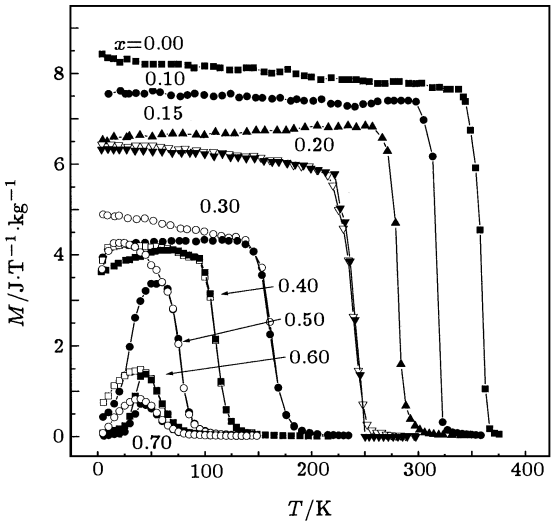


Fig.2. The M–T curves of the samples under zero magnetic field for $La_{0.7-x}Gd_xSr_{0.3}MnO_3$.

In order to explore the changes of magnetic structure at different doping contents, we measured the magnetic field dependence of magnetic moment (M–H curves) for $La_{0.7-x}Gd_xSr_{0.3}MnO_3$ (x=0.40, 0.50,

0.60 and 0.70) at 10 K ($\ll T_C$), as shown in Fig.3. For x=0.40, the M–H curve exhibits a good FM behaviour. When the magnetic field is larger than 0.02 T, the magnetic moment (M) tends to be saturated with increasing magnetic field, indicating that though the system is in a cluster state, the magnetic moments in the clusters turn to the same direction with increasing magnetic field. This phenomenon is called the spin-canted ferromagnetism state in some papers.[7] For x=0.60 and 0.70, the Gd content is high, so the Gd–O–Gd short-range order arrangement occurs and the Gd sublattice with the magnetism is formed in the La(Sr)–O plane, and the M–H curve does not show the behaviour like that in samples of $x \leq 0.50$ where the M first increases sharply then tends to be saturated. The M for x=0.60 and 0.70 increases slowly even under low magnetic fields and the M constantly increases with increasing H, but does not tend to be saturated, which is a typical AFM characteristic.[8] This implies that the magnetic moment of Gd^{3+} sublattice is anti-parallel to that of Mn^{3+}/Mn^{4+} sublattice. The sample with x=0.50 shows a transition from x=0.40 to x=0.60 and 0.70. At $H > 3$ T, the M–H curve is similar to that of x=0.40, and at $H < 1$ T, the M–H curve is similar to that of $x \geq 0.60$.

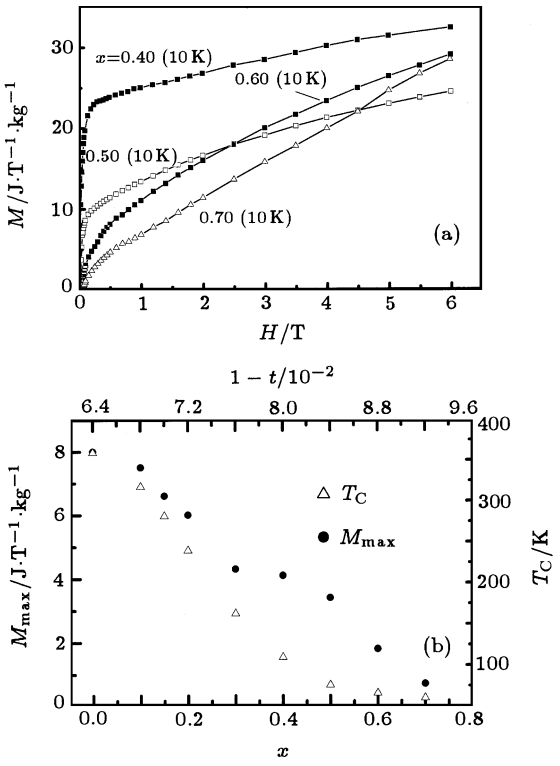


Fig.3. Field dependence of magnetization for some samples of $La_{0.7-x}Gd_xSr_{0.3}MnO_3$.

We choose Gd as the doping element for two reasons. First, Gd^{3+} ions have a larger magnetic moment ($\mu_{\rm eff} \approx 8.0\mu_B$), and it would increase T_C and strengthen M. Second, the radius $< r_{Gd} >$ of Gd ion is smaller than the $< r_{La} >$ of La ion, and this would decrease T_C and weaken M. Obviously, the interaction caused by Gd ion itself is a competitive factor for T_C and M. The magnetism of Gd benefits the phase transition from PM to FM, and the lattice distortion caused by the smallness of Gd ion radius $< r_{Gd} >$ will decrease T_C and weaken M. From Table 1, we find that the magnetism of the system is weakened and T_C decreases rapidly with increasing Gd doping content. Obviously, this can be attributed to the fact that the decrease of average rare-earth ion radius $< r_A >$ leads to the decrease of tolerance factor t and the distortion of bond length and angle of Mn–O–Mn, thus the double-exchange is depressed.[9,10] Figure 3(b) shows the relation between M, T_C and (1–t) or x (t is in a good linear relation with x). When $x \leq 0.30$, T_C and M decrease linearly with increasing (1–t), which means that the magnetism of Gd itself does not play an important role in the system, and that the decrease of average radius $< r_A >$ at A site changes the bond length and the angle of Mn–O–Mn, which dominate the T_C and M of the system. When $x \geq 0.40$, T_C and M do not show a linear relation with (1–t), indicating that T_C and M are influenced not only by the change of bond length and angle of Mn–O–Mn caused by Gd doping but also by the magnetic structure of the sublattice formed by Gd. Bokov *et al*[11] studied in detail the relation between the degree of lattice distortion and the intensity of magnetism. They found that when the lattice distortion is small, especially when $a = b \approx c$, all the samples exhibit ferromagnetic properties. And if a, b and c are very different from each other, the samples generally exhibit AFM or non-ferromagnetic property. This is in accordance with the conclusions stated above.

The change of magnetic structure is closely correlated with the Gd doping content. For $x \leq 0.20$, as the concentration of Gd is low, the system is dominated by the long-range ferromagnetic order of Mn–O–Mn, both PM–FM and IM transitions are in good accordance with the results reported previously. For x=0.30 and 0.40, the La–O–La(Sr) in La–O layer is ruptured by doping Gd ions which are distributed individually and randomly in La–O layer and the La(Sr)–O–Gd is formed, but the Gd–O–Gd correlation is not formed. The random magnetic potential and Coulomb potential of Gd ions make the long-

range order of Mn–O–Mn impossible, which results in Mn–O–Mn clusters, and forms a cluster-spin glass state. For $x \geq 0.50$, the Gd ions do not distribute themselves randomly in the La–O–La(Sr) layers as individual ions, but are arranged as Gd–O–Gd chains, and form the Gd–O–Gd sublattice together with the Mn–O–Mn sublattice, and an AFM structure between Mn–O–Mn and Gd–O–Gd is formed below T_C.

Table 1. T_C, T_C^{onset}, T_C(ESR), T_d, T_d(VRH) and T_0 in $La_{0.7-x}Gd_xSr_{0.3}MnO_3$ ($0.00 \leq x \leq 0.70$) samples.

x		0.0	0.10	0.15	0.20	0.30	0.40	0.50	0.60	0.70
T_C/K		360	318	282	240	163	110	76	66	60
T_C^{onset}/K		370	330	310	250	180	150	110	110	110
T_C(ESR)/K		370	330	310	280	180	170	110	110	100
T_d/K	thermally activated model				296	270	222	133		
	polaron model				285	244	217.6	117		
	VRH high temperature range				287	203	218	205	202	200
	VRH low temperature range				–	–	172–141	141–108	< 162	< 169
T_d(VRH)–T_C(ESR)/K	high temperature range				7	23	48	55	62	110
$T_0/10^7$K	high temperature range				0.767	5.35	7.13	15.5	23.4	16.5
	low temperature range				–	–	21.1	67.3	99.0	106

Note: T_C is the PM–FM transition temperature (that is at the minimum point of dM/dT), T_C^{onset} is the beginning temperature of PM–FM transition, T_C(ESR) is the temperature corresponding to the appearance of FM state in ESR spectra, T_d is the temperature where the fitted curve departs from the experimental curve, and T_0 is the parameter in VRH model.

The PM–FM transition of the Gd-doped system is obviously different from that of other doped systems. The magnetic transition of this system is very sharp, even in the cluster-spin glass state. In order to understand this phenomenon, we have studied the micromagnetism of the system by ESR spectra. Figures 4(a)–(i) give successively the ESR spectra of the samples with x=0.00, 0.10, 0.15, 0.20, 0.30, 0.40, 0.50, 0.60 and 0.70 respectively. Figure 4 shows that the samples with x=0.00, 0.10, 0.15, 0.20, 0.30, 0.40 and 0.50 exhibit single paramagnetic resonance lines (PRL) with $g \approx 2$ at the corresponding temperatures above 380, 340, 320, 290, 190, 175 and 120 K; and single ferromagnetic resonance lines (FRL) with $g > 2$ at the corresponding temperatures below those stated above. In Figs.4(e) and (f), the temperature where '△' is marked is the one corresponding to the appearance of FM state, that is T_C(ESR) in Table 1. The T_C(ESR) is just the T_C^{onset} which is the onset temperature corresponding to the occurrence of FM state in the M–T curve. These ESR lines are different from those reported previously; most reports indicate that there is a very wide temperature range for PM–FM transition. The ESR lines are double-line splitting from the PRL. That is to say, there are double peaks in the ESR spectra at the same temperature: one is the PRL and the other is the FRL in low fields. With decreasing temperature, the intensity of the PRL is gradually weakened, and the intensity of FRL is gradually strengthened and shifts to low fields. At a certain temperature the PRL disappears and there are only FRLs. For the $La_{0.7-x}Gd_xSr_{0.3}MnO_3$ system, there is no double-peak in the ESR line because the PM–FM transition has been accomplished within 10 K which is the temperature interval of ESR measurement. This also means that the magnetic transition of the $La_{0.7-x}Gd_xSr_{0.3}MnO_3$ system is really very sharp.

3.2. Phase separation

From Fig.3(b), we can see that the M decreases with increasing (1–t) or x, which means that the M does not contribute to the magnetism of Gd. The magnetism of the system is still dominated by DE interaction of Mn–O–Mn. From Table 1, we can see that the T_C^{onset} of the macroscopic magnetic moment for the system is in good accordance with the T_C(ESR) where the FM appears in ESR. This implies that the ESR line comes from Mn–O–Mn. It is interesting that the ESR lines of the samples with x=0.30 and 0.40 show a new phenomenon. Figure 4(e) shows that for the sample with x=0.30, a new bump besides the PRL line appears at 170–180 K which is above T_C (163 K).

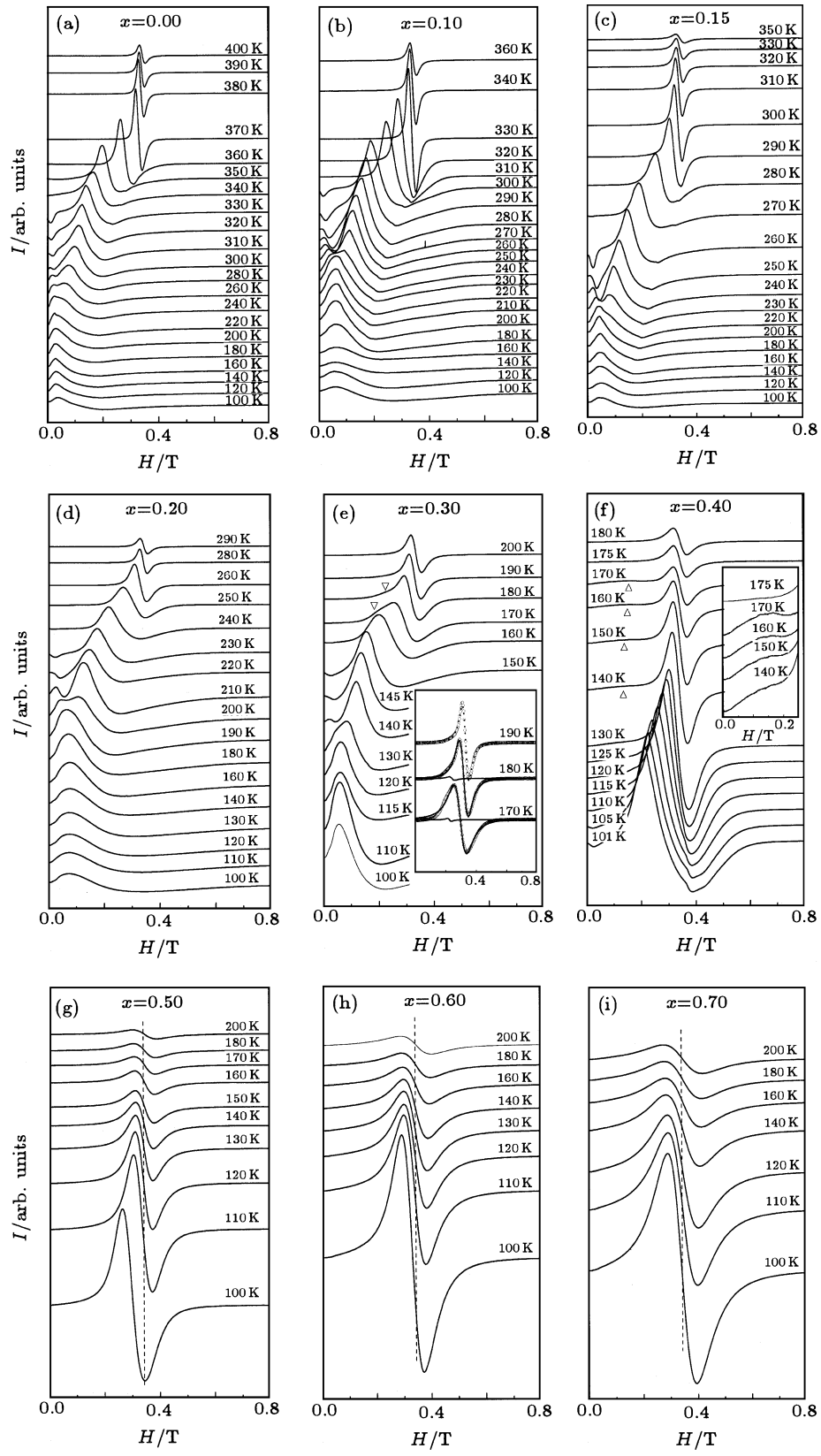


Fig.4. ESR spectra for samples $La_{0.7-x}Gd_xSr_{0.3}MnO_3$ (x=0.00, 0.10, 0.15, 0.20, 0.30, 0.40, 0.50, 0.60 and 0.70).

In the inset of Fig.4(e), we fit the experimental curves using double Lorentz lines. (The empty circles are experimental values, the dotted line is the fitting line of theory and experiment, and the solid lines are the double Lorentz lines). At 190 K, the experimental result is well fitted by a single PRL; but at 170–180 K, the double Lorentz lines are exhibited. One is PRL, the other is FRL. This means that the FM phases are separated from the PM phase.[12–15] Figure 4(f) shows that there also exists a bump in low magnetic fields besides the typical PRL at 140–170 K far above T_C(110 K) (see the inset of Fig.4(f)). All the above show that the FM phase appears in the PM phase for x=0.30 and 0.40.

For $x \geq 0.50$, $T_C < 76$ K, which lies out of the measurement range of our instrument (100–400 K), the ESR spectra in Figs.4(g)–(i) are single PRL at T≥110K, and the PRL shifts a little to the low field at 100 K, while no obvious phase separation is seen.

3.3. The influence of Gd doping on the resistance and transport behaviours

The $La_{0.7-x}Gd_xSr_{0.3}MnO_3$ system exhibits a complex magnetic structure with increasing Gd content. It is expected that there are different transport behaviours under different magnetic backgrounds. Figure 5 shows the ρ–T curves of samples with different Gd doping contents under zero magnetic field and 6 T field. It can be seen that corresponding to the above magnetic structures, there are three kinds of ρ–T relations: (1) For $x \leq 0.20$, the ρ–T curves below T_C exhibit a metal-like behaviour. (2) For x=0.30 and 0.40, though there is the IM transition in the ρ–T curves, the temperature corresponding to the IM transition peak is higher than the T_C, and the ρ–T curves on the two sides of the peak are nearly symmetrical; moreover, the temperature of the peak shifts gradually to low temperatures with increasing Gd doping. (3) For x=0.50, the resistivity is three orders of magnitude larger than that of samples with $x \leq 0.40$.

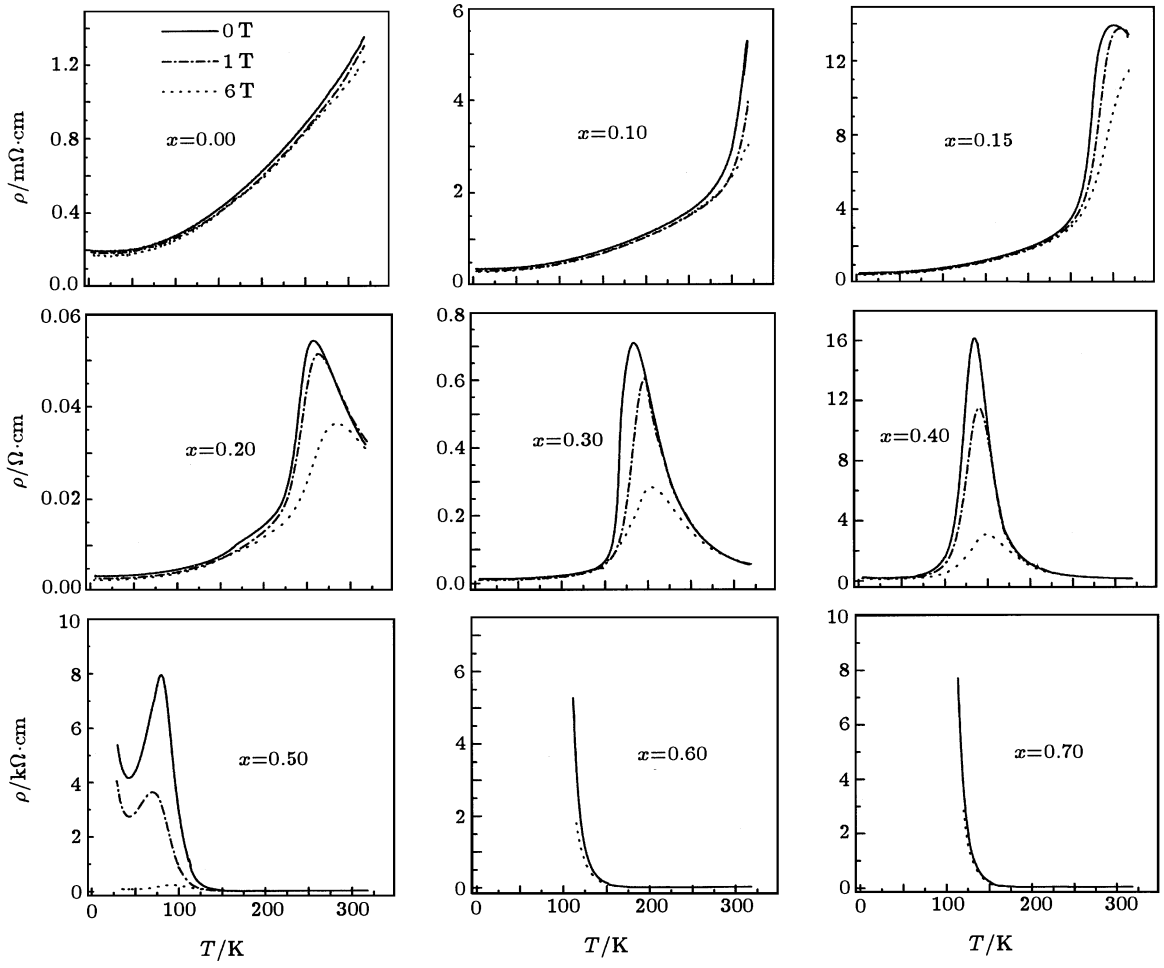


Fig.5. The ρ–T curves of the samples under zero field and magnetic field (H=1, 6 T) for $La_{0.7-x}Gd_xSr_{0.3}MnO_3$.

Though there is the IM transition above T_C, the ρ first increases and then decreases with decreasing temperature for $T < T_C$, and the ρ–T curve at low temperatures exhibits insulator-like behaviour again. This is seldom found in ABO_3 type CMR materials. Another new phenomenon is that for x=0.60 and 0.70, the ρ–T curve exhibits insulating behaviour even far above T_C though there is a magnetic transition. Obviously, these peculiar phenomena are closely connected with the magnetic structure of the system. For x=0.30 and 0.40, the random magnetic potential and Coulomb potential of Gd mainly destroy the Mn–O–Mn long-range order and thus form the Mn–O–Mn clusters. For $x \geq$0.50, the high-density random magnetic potential and Coulomb potential induced by Gd make the formation of Mn–O–Mn clusters impossible, and set e_g electrons in Mn–O–Mn in local state, so the samples with x=0.60 and 0.70 exhibit insulator behaviour in the temperature range far apart from the magnetic transition, and the resistance is beyond the measurement limit of our instruments. We continue to decrease the temperature to below T_C, but the resistance is still beyond the measurement limit. We guess that the FM arrangement of Mn–O–Mn sublattice is anti-parallel to one of the Gd sublattices below T_C, therefore the motion of e_g electrons under the AFM potential which results in the Gd sublattice, is of insulating behaviour. For x=0.50, the abnormal change of ρ–T curve also is connected with its transition from the cluster-spin glass state to AFM state. At $T > 20$ K, the ρ–T curve is in accordance with that of the cluster-spin glass state (x=0.30 and 0.40), while at $T < 20$ K, the system has transited into the AFM state, the carriers move under the AFM background and the ρ–T curve shows insulating behaviour again, which causes the increase of ρ after its decrease with decreasing temperature at low temperatures.[16,17]

In order to investigate the semiconductor-like or insulator-like transport behaviours of the samples, we fit the ρ–T curves under zero field for the samples with $x \geq$0.20 by using the thermally activated model $\rho(T) = \rho_0 \exp(E/k_B T)$, the small polaron activated model $\rho(T) = \rho_0 T \exp(E_P/k_B T)$, and the VRH model $\rho(T) = \rho_0 \exp(T_0/T)^{1/4}$, as shown in Fig.6; the fitting parameters are listed in Table 1. Figure 6 shows that for samples with 0.20$\leq x \leq$0.40, the temperature range in which the polaron model fits the experimental is a little different from that obtained using the VRH model; and for $x \geq$0.50, the polaron model seems to be better than the VRH model, but the activated energies E_P of the samples with x=0.30, 0.40 and $x \geq$0.50 are respectively 145, 148 and $\geq$162 meV, and these values are obviously too large, so the VRH model is more reasonable.[18] For the Mn–O–Mn cluster state induced by Gd doping, the VRH induced by Gd doping probably comes from two aspects. On one hand, the Gd doping causes not only clusters but also random distribution of the local spin in PM state in

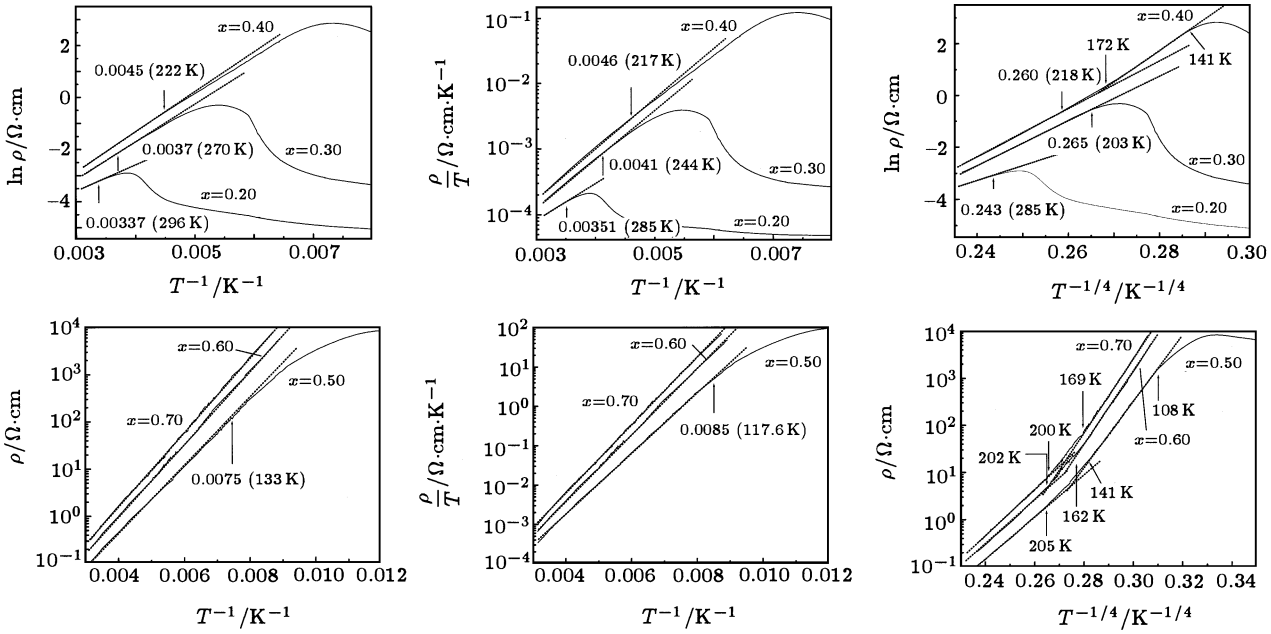


Fig.6. The fitted curves by using the three models for $La_{0.7-x}Gd_xSr_{0.3}MnO_3$.

the clusters, so random magnetic potential is formed and the VRH environment is produced; on the other hand, the transport of e_g electrons between clusters is obviously of VRH which forms naturally. If the contribution of the latter to the resistance is larger than that of the former, the resistivity will be dominated by VRH between clusters at $T < T_C$. But the ρ–T curves in Fig.5 show that for the samples with x=0.30 and 0.40, the PM–FM transition occurs along with IM transition, and the ρ–T curves exhibit a metal behaviour at $T < T_C$. This indicates that the VRH conduction in PM state is mainly dominated by the scattering in the inhomogeneous PM state inside the cluster. For high Gd doping, the behaviour of e_g electrons is so strange that the ρ–T relation obeys the VRH law in the two temperature ranges.

3.4. Abnormal transport behaviour in heavily doped specimens

From Figs.5 and 6, it can be seen that there are two unusual aspects of the transport behaviour. First, for the samples with x=0.30 and 0.40, Figs.5(e) and (f) show that the temperature of IM transition is higher than that of PM–FM transition. Second, for the samples with x=0.40, 0.50, 0.60 and 0.70 in Fig.6, the experimental data fit well to the VRH model not only in the high temperature range above T_d's(VRH)=218, 205, 202, 200 K, but also in the low temperature range 172–141 K, 141–108 K, < 162 K and < 169 K (T_d's(VRH) are the temperatures where the experimental results depart from the fitting lines, and they are all higher than T_C). However, the slopes of the fitting lines in the low temperature range are higher than those in the high temperature range. From Table 1, we can see that for samples with x=0.30 and 0.40, the phase separation takes place at temperatures 180 and 170 K, respectively, and the FM phase is separated from the PM phase at these temperatures. The IM transition occurs along with the phase separation, so the temperature of IM transition is higher than that of PM–FM transition. Additionally, Fig.3(b) and Table 1 show that for samples with $x \geq$0.50, T_C and M do not decrease linearly with increasing x, whereas T_d(VRH)-T_C(ESR) increases quickly with x. This implies that the magnetic and electric behaviours of the system are not only dependent on the tolerance factor t, but also correlated with the magnetic structure of the Gd–O–Gd sublattice. It is known that the Gd^{3+} sublattice is anti-parallel to the Mn^{3+}/Mn^{4+} sublattice, implying the existence of possible FM state in Gd–O–Gd sublattice. We deduce that at high doping level, the Gd–O–Gd sublattice forms a FM state at first, then induces the formation of FM state in Mn–O–Mn sublattice. This FM state is formed earlier than that caused by t. The temperature where the FM transition appears in Gd sublattice is T_d(VRH). Since the magnetism of the Gd–O–Gd is weak, the M for x=0.70 is much smaller than that for x=0.00 (Fig.2), and the PM–FM transition is still dominated by Mn–O–Mn for x=0.70. In ESR measurements the magnetism of Gd sublattice also does not exhibit, because it is much weaker than that of Mn–O–Mn sublattice. However, the FM of Gd sublattice induces the PM–FM transition of Mn–O–Mn to take place at higher temperature. As a result, T_C and M are higher than the linearly extrapolated values in the T_C and M versus (1–t) relations. At different temperatures, there are different arrangements of magnetic moments in the Gd–O–Gd sublattice, which is why the fits of resistivity data to VRH for samples with x=0.40, 0.50, 0.60 and 0.70 are divided into two temperature ranges. The fitting results in Fig.6 show that in the high temperature range above T_d(VRH), the Gd^{3+} sublattice is in a PM state, and the random magnetic potential of Gd contributes to the VRH background. Therefore, the transport behaviour obeys the VRH law. Interestingly, their ρ-$T^{-1/4}$ curves in the high temperature range are nearly parallel. Table 1 shows that their T_0 are close to each other, which indicates that with increasing Gd content, the sizes of the Gd–O–Gd clusters are almost the same, e.g. the Gd^{3+} sublattice makes a homogeneous random magnetic background. The sample with x=0.40 exhibits a phase separation in which the FM clusters are formed, causing a strong magnetic-potential scattering on the e_g electrons, so the e_g electrons become localized and the transport obeys the VRH law below 170 K with a steep slope. For higher doped samples, the ESR results show that the ESR line with $g \approx 2$ appears at $T >$ 110 K for x=0.50 in Fig.4(g), and the g value is a little larger than 2 at $T \approx$ 100 K. For x=0.60 and 0.70 the g value deviates a little from 2 only at 100 K, and the phase separation does not occur (see Figs.4(h) and (i)), which indicates again that the distribution of Gd ions is very homogeneous so that the Mn–O–Mn cannot form clusters. This is also proved in Figs.2(g)–(i). However, we should emphasize that even for x=0.70, the Gd atoms have replaced La atoms totally, yet 30% Sr in the Gd layer is still sufficient to divide the Gd–O–Gd

sublattice into randomly distributed magnetic clusters. The magnetic state (PM or FM) in the clusters contributes to the random magnetic potential. For x=0.50 and 0.60, La and Sr atoms divide the Gd–O–Gd sublattice into more randomly distributed clusters, and the cluster size is smaller than that for x=0.70. In the PM state, the magnetic moments of Gd in these clusters are arranged randomly, and form a relatively homogeneous magnetic-random-potential background. Below T_d(VRH), the clusters of Gd turn into a FM state. The magnetic potential of the FM state is stronger than that of the PM state, and the e_g electrons are more localized, leading to a relatively larger T_0. With increasing x, the FM state is strengthened and causes the magnetic potential to be stronger. Therefore, below the temperatures 141, 162 and 169 K, the transport behaviour obeys the VRH law and T_0 increases gradually, which is just the result shown in Table 1.

3.5. CMR effects

Figure 5 shows that the resistivity peak is reduced under a magnetic field. Two factors are known to cause the influence of magnetic field on the CMR materials: namely, the thermal fluctuation and the magnetic moments in the FM state. The former can be depressed by the applied magnetic field so that the PM–FM transition occurs at high temperatures, which means that the IM transition temperature T_p shifts to a higher temperature. The latter results in a more ordered FM state at the same temperature and reduces the scattering on the carriers, so that the resistivity in a magnetic field is lower than that in zero field. These two factors lead to CMR effects.

Figure 7 shows the relationship between the magnetoresistance MR and temperature T in the $La_{0.7-x}Gd_xSr_{0.3}MnO_3$ system. Here the MR is defined as follows:

$$\mathrm{MR}(\%) = \frac{\rho(0) - \rho(H)}{\rho(H)} \times 100\%.$$

From Fig.7, it can be seen that for the samples in which there occurs IM transition (i.e. samples with $x \leq 0.50$), the MR exhibits a peak near T_C, the peak intensity of it increases rapidly with increasing Gd

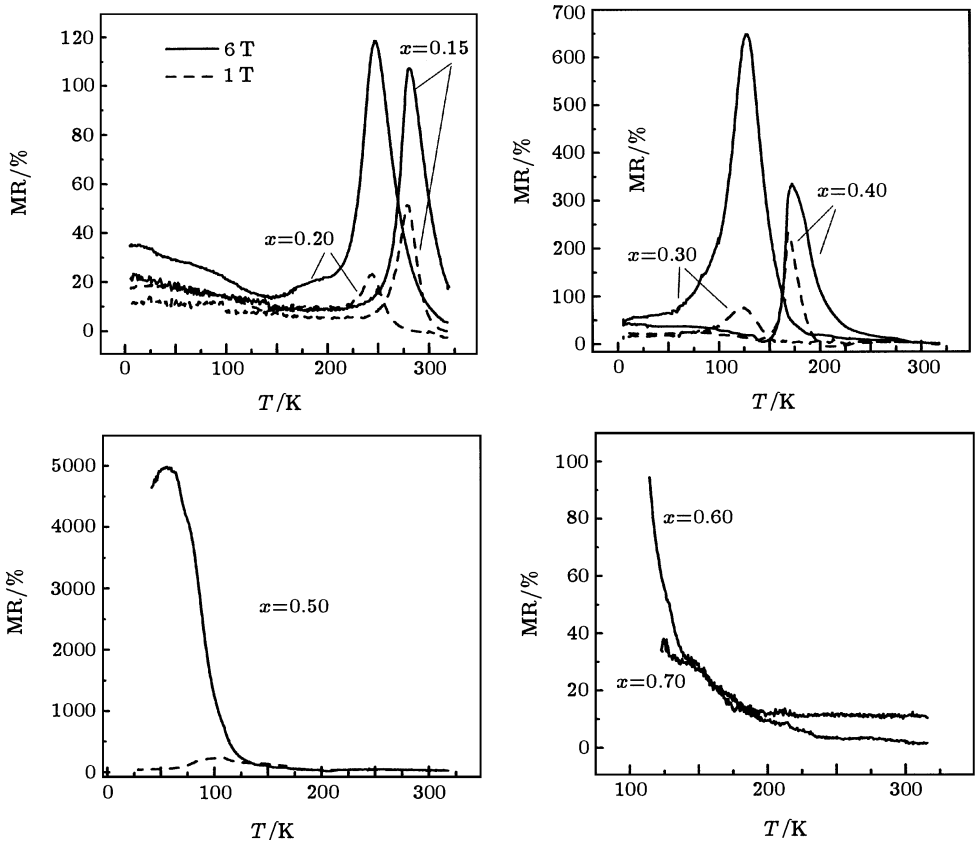


Fig.7. The temperature dependence of magnetoresistance MR for $La_{0.7-x}Gd_xSr_{0.3}MnO_3$.

doping. For the sample with x=0.50, the maximum MR value is 5000% at 6 T. Even at 1 T magnetic field, the maximum MR value reaches 200%. From Figs.5 and 7, we also notice that the sensitivity of MR to the magnetic field increases with Gd doping. For example, the resistivity under 1 T magnetic field is very different from that under 6 T for the sample with x=0.50. This is attributed to the fact that the AFM order cannot exist under 6 T magnetic field and the insulator behaviour at low temperatures is depressed, so that the resistivity decreases rapidly. For the samples with x=0.60 and 0.70, the insulator behaviour emerges in the temperature range apart from the magnetic transition so that the MR is small and is nearly independent of the magnetic field.[19]

4. Conclusions

In this paper, the influences of Gd doping at the A site on the magnetism and transport behaviours in the $La_{0.7-x}Gd_xSr_{0.3}MnO_3$ system have been studied. The following conclusions are obtained:

(1) The system is in a long-range FM order state when the Gd doping content is low. For x=0.30 and 0.40, the samples display a cluster-spin glass behaviour. For $x \geq$0.50, the system exhibits an AFM state at low temperatures.

(2) With increasing Gd doping, the transport mechanism changes from the polaron hopping to the VRH. The VRH background in the high-temperature range comes from the random magnetic potential due to the random distribution of Gd ions, and it comes from the magnetic connection due to FM arrangement of Gd sublattice in the low-temperature range.

(3) With heavy doping, the transport behaviour becomes abnormal due to complex magnetic background, the ρ–T curves obey the VRH law with different T_0 in the two temperature ranges.

References

[1] Helmolt R V, Wecker J, Holzapfel B *et al* 1993 *Phys. Rev. Lett.* **71** 2331
[2] Pi L, Xu X J and Zhang Y H 2000 *Phys. Rev.* B **62** 5667
[3] Liu X M, Xu X J and Zhang Y H 2000 *Phys. Rev.* B **62** 5112
[4] Deteresa J M *et al* 1996 *Phys. Rev. Lett.* **76** 3392
[5] Liu N, Sun Y and Zhang Y H 2001 *Chin. Phys. Lett.* **18** 957
[6] Sun Y, Xu X J, Zheng L *et al* 1996 *Phys. Rev.* B **60** 12317
[7] Guo Z B, Huang H, Ding W P *et al* 1997 *Phys. Rev.* B **56** 10789
[8] Snyder G J, Booth C H, Bridges F *et al* 1997 *Phys. Rev.* B **55** 6453
[9] Hwang H Y, Cheong S W, Radaelli P G *et al* 1995 *Phys. Rev. Lett.* **75** 914
[10] Fpontcuberta J, Martinez B, Seffar A *et al* 1996 *Phys. Rev. Lett.* **76** 1122
[11] Bokov V A, Grigoryan N A, Bryzhina M F *et al* 1968 *Phys. Status Solidi* **28** 835
[12] Zheng L, Xu X J, Pi L *et al* 2000 *Phys. Rev.* B **62** 1193
[13] Moreo A, Yunoki S and Dagotto E 1999 *Science* **283** 2034
[14] Fath M, Freisem S, Menovsky A A *et al* 1999 *Science* **285** 1540
[15] Uehara M, Mori S, Chen C H *et al* 1999 *Nature* **399** 560
[16] Wang Z H *et al* 1999 *Acta Phys. Sin.* **48** 757 (in Chinese)
[17] Li G *et al* 1999 *Acta Phys. Sin.* **48** 505 (in Chinese)
[18] Mott N F and Davies E A 1971 *Electronic Processes in Noncrystalline Materials* (Oxford: Oxford University Press)
[19] Dagotto E, Hotta T and Moreo A 2001 *Phys. Rep.* **344** 1